Plasmons in imperfect parabolic quantum-well wires: Self-consistent calculations

L. Wendler
Fachbereich Physik, Martin-Luther-Universität Halle, Friedemann-Bach-Platz 6, D-06108 Halle, Germany

R. Haupt
Institut für Festkörpertheorie und Theoretische Optik, Friedrich-Schiller-Universität Jena, Max-Wien-Platz 1, D-07743 Jena, Germany

(Received 19 April 1995)

The effects of deviations from the bare perfect parabolic confining potential of a quantum-well wire on the dispersion relations of quasi-one-dimensional plasmons are studied. We calculate self-consistently the ground state in the Hartree approximation and the density response in the random-phase approximation. We find that for a bare perfect parabolic potential, one intersubband mode, the fundamental or Kohn's mode, is pinned at the bare harmonic oscillator frequency independent from the electron density. It is shown that small nonparabolic imperfections shift the fundamental mode to higher or smaller frequencies and depend on the electron density.

I. INTRODUCTION

Synthetic low-dimensional electron systems are presently a subject of enormous interest. Much insight into the electronic properties of such electron systems is gained from optical investigations, i.e., from *far-infrared* (FIR) *transmission spectroscopy* and *resonant inelastic light scattering*. Quantum confinement of the electrons in two spatial directions results in *quantum-well wires* (QWW's), in which the electrons are only free in one spatial direction. The most important collective excitations of the quasi-one-dimensional (Q1D) electron system, synthesized in a QWW, are the *plasmons*. Their spectrum depends characteristically on the properties of the quasi-one-dimensional electron gas (Q1DEG).

Q1D plasmons have been investigated theoretically[1–14] and experimentally[15–26] in isolated QWW's and lateral multiwire superlattices. Caused by the size quantization, the excitation spectrum is split in *intrasubband* and *intersubband excitations*. The intersubband plasmons have frequencies above the corresponding single-particle transition frequency for usual electron number densities. This frequency shift is a measure of the strength of the Coulomb interaction. Within the *random-phase approximation* (RPA) this frequency shift results from resonance screening and is called *depolarization shift*. Optical investigations of QWW's have demonstrated that in etched[27] and field-effect samples,[28] the bare confining potential V_0 is of parabolic shape in a good approximation. In the case of a perfect parabolic potential, the generalized Kohn's theorem[29,30] predicts that in a FIR experiment, the Q1DEG absorbs radiation only at the bare harmonic oscillator frequency, independent of the electron-electron interaction and the number of electrons in the QWW. This *intersubband resonance* (*dimensional resonance*) is called the *fundamental mode* (or *Kohn's mode*) and corresponds to the center-of-mass motion of all confined electrons. In the presence of nonparabolicity of the confining potential, besides the fundamental mode, higher intersubband resonances become visible.[22,26] For this reason, optical measurements are useful in characterizing departures from ideal parabolicity in experimental samples. In agreement with Kohn's theorem, it has been shown[11] for a bare (initial) perfect parabolic confining potential that a self-consistent calculation of the ground state and the response of a Q1DEG results in a frequency of the lowest intersubband plasmon, which is nearly identical to the bare harmonic oscillator frequency and independent from the density of the Q1DEG for nearly vanishing wave vector. Only this mode is dipole active. Increasing wave vector results in an increasing frequency of this mode and a redistribution of the FIR oscillator strengths, i.e., higher modes become also dipole active.

The aim of this present work is to study how the dispersion relations of the Q1D plasmons in QWW's change from the perfect parabolic case, when different imperfections are present. The work is performed by self-consistent calculations of the ground state and the response in the framework of the Hartree approximation and the RPA, respectively.

II. GROUND STATE

The model used in this paper is the following. The electrons are totally confined in an effective potential $V_{\text{eff}}(\mathbf{x}) = V_{\text{eff}}(y) + V_{\text{eff}}(z)$ assumed separated for the y and z direction, which is within the Hartree approximation a sum of the bare potential $V_0(\mathbf{x})$, resulting from the tailoring of the conduction-band edge and a possible applied external electrostatic potential. Because in the experimental realized samples the potential in the growth direction (z direction) is very narrow in comparison to the width of the potential in the lateral direction (y direction), we can study the QWW by a model in which the electrons are confined in a zero-thickness x-y plane along the z direction at $z = 0$. The electrostatic

potential $\Phi(\mathbf{x})$ is a solution of

$$\nabla \cdot [\varepsilon_s(\mathbf{x})\, \nabla\Phi(\mathbf{x})] = \frac{e}{\varepsilon_0}\,[n_0(\mathbf{x}) - N_D^+(\mathbf{x})]\,, \tag{1}$$

where $n_0(\mathbf{x}) = n_0(y)\delta(z)$ is the electron number density of the ground state, $N_D^+(\mathbf{x}) = N_D^+(z)$ is the density of the positive charges, necessary to maintain charge neutrality, $\varepsilon_s(\mathbf{x})$ is the background static dielectric constant, ε_0 the permittivity in vacuum, and the electron charge is $-e$. Neglecting image effects in Eq. (1) and assuming that the length of the wire L_x is very large, the Hartree potential $V_H(y) = -e\Phi(y)$ is given by

$$V_H(y) = \frac{e^2}{2\pi\varepsilon_0\varepsilon_s}\int_{-\infty}^{\infty} dy' n_0(y') \ln\frac{y_0}{|y-y'|}\,, \tag{2}$$

where y_0 is a free constant, to which this potential is determined. With respect to the translational symmetry in the x direction and the assumed separation of the effective potential, the motion of the electrons separates. The wave functions and eigenvalues are given by

$$\langle \mathbf{x}|Lk_x\rangle = \Psi_{Lk_x}(\mathbf{x}) = \frac{1}{\sqrt{L_x}}\, e^{ik_x x}\, \xi_L(y)\, \varphi(z);$$
$$|\varphi(z)|^2 = \delta(z)\,, \tag{3}$$

$$\mathcal{E}_L(k_x) = \mathcal{E}_L + \frac{\hbar^2 k_x^2}{2m_e}\,; \quad L = 0,1,2,3,\ldots\,. \tag{4}$$

In the following, we suppose spin degeneracy and omit the spin index. In the above expressions, k_x is the wave vector component in x direction and m_e is the effective conduction-band-edge mass of the electrons. The subband energies $\mathcal{E}_L$ and the envelope wave function $\xi_L(y)$ are obtained from the one-dimensional Schrödinger equation,

$$\left(-\frac{\hbar^2}{2m_e}\,\frac{d^2}{dy^2} + V_{\text{eff}}(y)\right)\xi_L(y) = \mathcal{E}_L\,\xi_L(y)\,, \tag{5}$$

where $V_{\text{eff}}(y) = V_0(y) + V_H(y)$, $V_H(y)$ is given by Eq. (2) and $n_0(y) = \sum_L n_0^{(L)}(y)$, with

$$n_0^{(L)}(y) = \frac{4}{\pi\hbar}\sqrt{\frac{m_e}{2}}|\xi_L(y)|^2\sqrt{E_F - \mathcal{E}_L}\;\Theta(E_F - \mathcal{E}_L)\,. \tag{6}$$

In this equation, $n_0^{(L)}(y)$ is the contribution of the Lth subband to the electron number density $n_0(y)$, $\Theta(x)$ is the Heaviside unit step function with $\Theta(x) = 1$ for $x > 0$ and $\Theta(x) = 0$ for $x < 0$. The Fermi energy E_F is determined from the 1D electron number density (number of electrons per unit length) $n_{1\text{DEG}} = \sum_L n_{1\text{DEG}}^{(L)}$, where

$$n_{1\text{DEG}}^{(L)} = \frac{4}{\pi\hbar}\sqrt{\frac{m_e}{2}}\sqrt{E_F - \mathcal{E}_L}\;\Theta(E_F - \mathcal{E}_L) \tag{7}$$

is the number of electrons per unit length in the Lth subband. The Fermi wave vectors of the different subbands are given by

$$k_F^{(L)} = \begin{cases} \sqrt{2m_e(E_F - \mathcal{E}_L)/\hbar^2} & \text{if} \quad E_F > \mathcal{E}_L \\ 0 & \text{if} \quad E_F \le \mathcal{E}_L, \end{cases} \tag{8}$$

and the corresponding Fermi velocities are $v_F^{(L)} = \hbar k_F^{(L)}/m_e$. The self-consistent solution of Eqs. (5), (6), (7), and (2) gives the subband energies, the charge-density profile, the Fermi energy, and the effective potential. For the bare potential, we use

$$V_0(y) = V_p(y) + V_{\text{np}}(y), \tag{9}$$

with the perfect parabolic part

$$V_p(y) = \frac{m_e\Omega^2}{2}y^2, \tag{10}$$

and the deviation, i.e., the nonparabolic part

$$V_{\text{np}}(y) = A_3y^3 + A_4y^4 + A_5y^5 + A_6y^6\,. \tag{11}$$

To perform the self-consistent calculations of the ground state, the envelope wave function is represented by the closure set of wave functions $\xi_L^{(0)}(y)$,

$$\xi_L(y) = \sum_{L'=0}^{\infty} C_{LL'}\xi_{L'}^{(0)}(y)\,, \tag{12}$$

where $\{\xi_L^{(0)}(y)\}$ are the eigenfunctions of Eq. (5) with $V_{\text{eff}}(y) = V_p(y)$ and are given by

$$\xi_L^{(0)}(y) = \frac{1}{(2^L L!\,\pi^{1/2}l_\Omega)^{1/2}}\,\exp\left(-\frac{y^2}{2l_\Omega^2}\right)\,H_L\left(\frac{y}{l_\Omega}\right)\,. \tag{13}$$

Herein, $H_L(y)$ is the Hermite's polynomial and $l_\Omega = [\hbar/(m_e\Omega)]^{1/2}$. The corresponding eigenvalues read

$$\mathcal{E}_L^{(0)} = \hbar\Omega(L + \tfrac{1}{2})\,; \quad L = 0,1,2,\ldots\,. \tag{14}$$

Using Eq. (12) in the Schrödinger equation, Eq. (5), and multiplying this equation from the left with $\xi_{L''}^{(0)}(y)$ and subsequently integrate it over y, we recover the eigenvalue equation,

$$\sum_{L'} C_{LL'}[(\mathcal{E}_L - \mathcal{E}_{L'}^{(0)})\delta_{L'L''} - V_{L''L'}^H - V_{L''L'}^{\text{np}}] = 0\,, \tag{15}$$

where

$$V_{L''L'}^H = \int_{-\infty}^{\infty} dy\, \xi_{L''}^{(0)}(y)\, V_H(y)\, \xi_{L'}^{(0)}(y),$$

$$V_{L''L'}^{\text{np}} = \int_{-\infty}^{\infty} dy\, \xi_{L''}^{(0)}(y)\, V_{\text{np}}(y)\, \xi_{L'}^{(0)}(y)\,. \tag{16}$$

The matrix elements of the Hartree potential are given by

$$V^H_{L_1L_2} = \frac{\sqrt{2m_e}\,e^2}{\pi^2\hbar\varepsilon_0\varepsilon_s}\sum_L \Theta(E_F-\mathcal{E}_L)\sqrt{E_F-\mathcal{E}_L} \times \sum_{L',L''} C_{LL'}C_{LL''}f^H_{L'L''L_1L_2}\,, \tag{17}$$

where the form factor reads

$$f^H_{L_1L_2L_3L_4} = \int_{-\infty}^{\infty}dy\int_{-\infty}^{\infty}dy'\,\xi^{(0)}_{L_1}(y)\,\xi^{(0)}_{L_2}(y) \times \ln\frac{y_0}{|y-y'|}\,\xi^{(0)}_{L_3}(y')\,\xi^{(0)}_{L_4}(y')\,. \tag{18}$$

For $L_1 \geq L_2$, the matrix elements of the nonparabolic part of $V_0(y)$ are given by

$$\begin{aligned}
V^{\rm np}_{L_1L_2} = {} & A_3\left(\frac{l_\Omega}{\sqrt{2}}\right)^3[3L_1^{3/2}\delta_{L_2,L_1-1}+\sqrt{L_1(L_1-1)(L_1-2)}\delta_{L_2,L_1-3}] \\
& +A_4\left(\frac{l_\Omega}{\sqrt{2}}\right)^4[6(L_1^2+L_1+1/2)\delta_{L_2,L_1}+4(L_1-1/2)\sqrt{L_1(L_1-1)}\delta_{L_2,L_1-2} \\
& +\sqrt{L_1(L_1-1)(L_1-2)(L_1-3)}\delta_{L_2,L_1-4}] \\
& +A_5\left(\frac{l_\Omega}{\sqrt{2}}\right)^5[10(L_1^2+1/2)\sqrt{L_1}\delta_{L_2,L_1-1}+5(L_1-1)\sqrt{L_1(L_1-1)(L_1-2)}\delta_{L_2,L_1-3} \\
& +\sqrt{L_1(L_1-1)(L_1-2)(L_1-3)(L_1-4)}\delta_{L_2,L_1-5}] \\
& +A_6\left(\frac{l_\Omega}{\sqrt{2}}\right)^6[20(L_1^3+3/2L_1^2+5/2L_1+3/4)\delta_{L_2,L_1}+15(L_1^2-L_1+1)\sqrt{L_1(L_1-1)} \\
& \times\delta_{L_2,L_1-2}+6(L_1-3/2)\sqrt{L_1(L_1-1)(L_1-2)(L_1-3)}\delta_{L_2,L_1-4} \\
& +\sqrt{L_1(L_1-1)(L_1-2)(L_1-3)(L_1-4)(L_1-5)}\delta_{L_2,L_1-6}]\,.
\end{aligned} \tag{19}$$

Because the potential $V_0(y)$ is infinitely high, the wave functions $\xi^{(0)}_L(y)$ are real and hence, $V^H_{LL'} = V^H_{L'L}$ and $V^{\rm np}_{LL'} = V^{\rm np}_{L'L}$ are valid. From Eq. (15), the renormalized single-particle subband energies $\mathcal{E}_L$ follow as solutions of the determinantel equation,

$$\det[(\mathcal{E}_L-\mathcal{E}^{(0)}_{L'})\delta_{L'L''}-V^H_{L''L'}-V^{\rm np}_{L''L'}] = 0\,. \tag{20}$$

For the numerical calculations throughout this paper, we assume a QWW prepared on a GaAs–$Ga_{1-x}Al_xAs$ heterojunction with the material parameters for GaAs: $\varepsilon_s = 12.87$, $m_e = 0.06624m_0$, where m_0 is the bare electron mass and $\hbar\Omega = 2$ meV. Further, we assume that the effective confining potential is mirror symmetric at the plane $y = 0$, which is the typical case for experimentally realized samples. Hence, we have $A_3 = A_5 = 0$ in Eq. (11) and we use the boundary condition $\partial/\partial y V_{\rm eff}(y)|_{y=0} = 0$. The free constant y_0 is chosen in such a manner that the Fermi energy is $E_F = 0$ as a reference level without loss of generality.

Figure 1 shows the different bare potentials considered in the following for the self-consistent calculations. We consider two types of deviations from the perfect parabolic potential: (i) $A_4 > 0$ and $A_6 = 0$, which effectively narrows the well and (ii) $A_4 < 0$ and $A_6 = 0.1668\,l_\Omega^2A_4^2/(\hbar\Omega) - 0.058\,32\,A_4/l_\Omega^2 > 0$ is chosen to design the bare potential with a flatter bottom.

In Fig. 2 we show the renormalized subband energies as a function of the electron density in the QWW for three different bare potentials. For $A_4 > 0$, the increase of the nonparabolicity increases the intersubband separation, and the onset of the occupation of a subband is

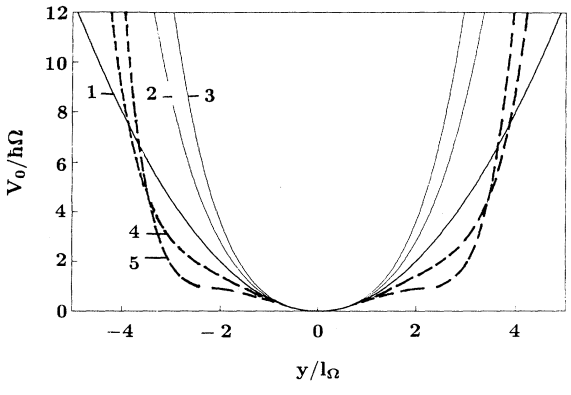

FIG. 1. Bare potentials $V_0(y)$ used in the self-consistent calculations: (1) bare perfect parabolic potential (heavy solid line), $A_4 = A_6 = 0$ and bare nonparabolic potentials, $A_4 > 0, A_6 = 0$ (thin solid lines); (2) $A_4 = 0.05\,\hbar\Omega/l_\Omega^4$; (3) $A_4 = 0.1\,\hbar\Omega/l_\Omega^4$ and $A_4 < 0, A_6 > 0$ (dashed lines); (4) $A_4 = -0.05\,\hbar\Omega/l_\Omega^4$, $A_6 = 0.00333\,\hbar\Omega/l_\Omega^6$; (5) $A_4 = -0.1\,\hbar\Omega/l_\Omega^4$, $A_6 = 0.0075\,\hbar\Omega/l_\Omega^6$.

shifted to higher electron densities. For $A_4 < 0$, the effect of the nonparabolicity on the subbands is twofold: (i) for lower subbands the subband energy spacing decreases but (ii) for higher subbands the subband energy spacing increases. The occupation of the subbands starts at nearly the same electron density as for the bare perfect parabolic potential.

In Fig. 3, we show the subband energies as a function of A_4 for three different electron densities. It is seen that the nonparabolicity of the bare potential influences the higher subbands stronger than the lowest-lying subbands. Further, the deviation with $A_4 > 0$ induces much more change in the subband energies. This increases with increasing electron density.

Figure 4 shows the charge-density profiles for the different bare potentials and different electron densities. It is seen that for $A_4 > 0$ the effect of the nonparabolicity is to broaden the charge-density profile for small electron

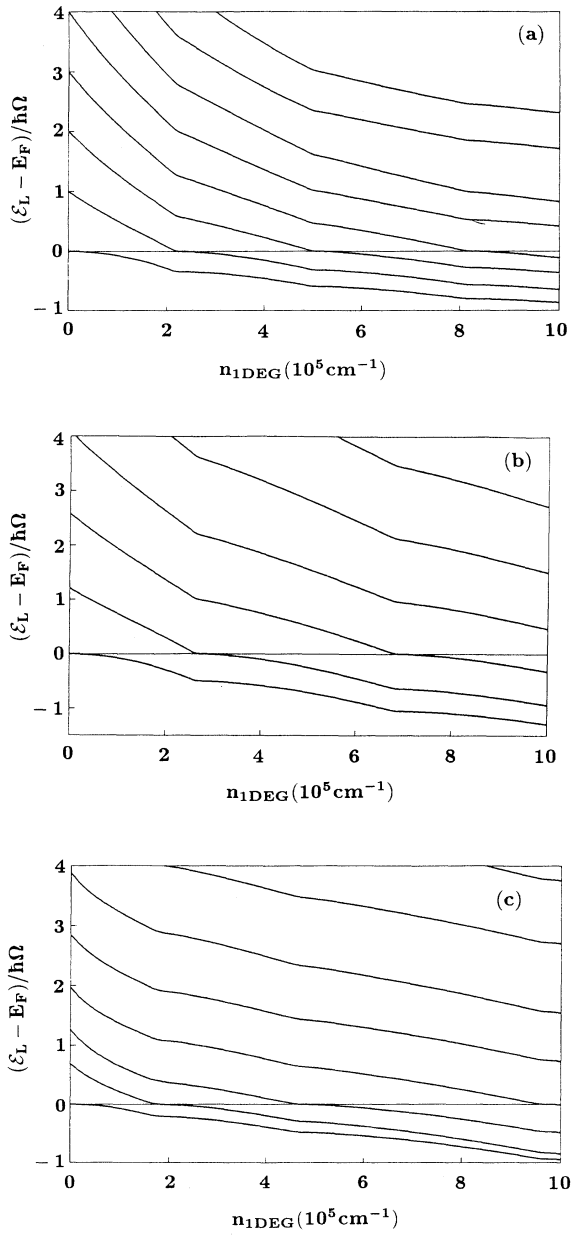

FIG. 2. Subband energies as a function of the electron density in the QWW measured from the Fermi energy: (a) $A_4 = A_6 = 0$; (b) $A_4 = 0.1\,\hbar\Omega/l_\Omega^4$, $A_6 = 0$; (c) $A_4 = -0.1\,\hbar\Omega/l_\Omega^4$, $A_6 = 0.0075\,\hbar\Omega/l_\Omega^6$. The parameters of the QWW are given in the text.

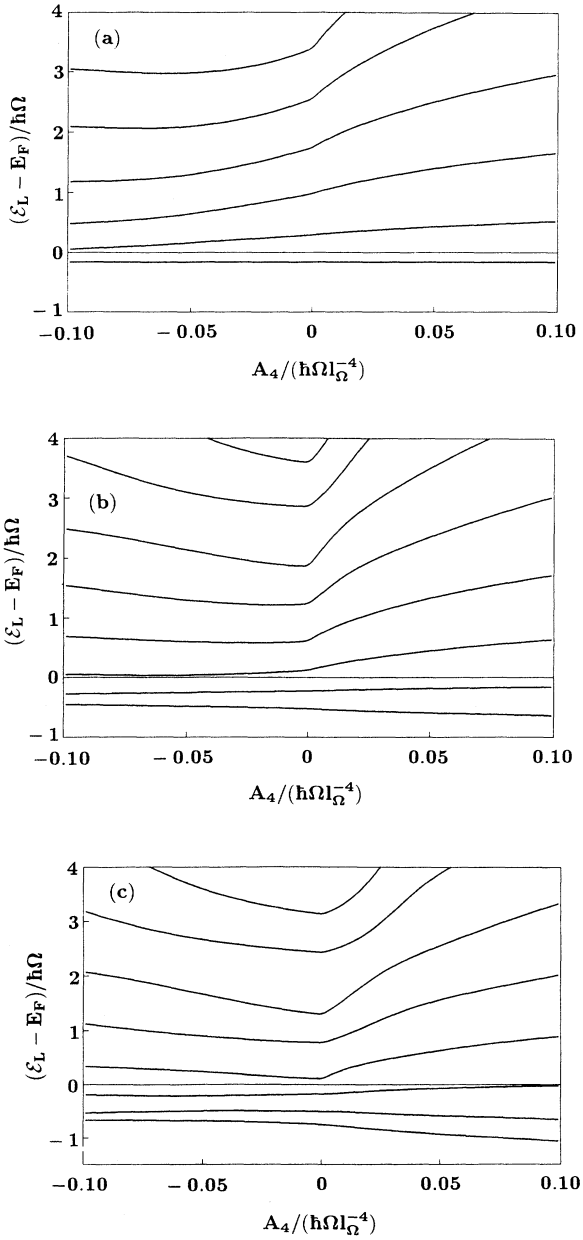

FIG. 3. Subband energies as a function of the strength of the nonparabolicity parameter A_4 with $A_6 = 0$ for $A_4 > 0$ and $A_6 = 0.1668\,l_\Omega^2 A_4^2/(\hbar\Omega) - 0.05832\,A_4/l_\Omega^2$ for $A_4 < 0$ for the electron number densities: (a) $n_{1DEG} = 1.5 \times 10^5$ cm^{-1}, (b) $n_{1DEG} = 4.5 \times 10^5$ cm^{-1}, and (c) $n_{1DEG} = 7.5 \times 10^5$ cm^{-1}.

densities, where one and two subbands are occupied and for higher electron densities the quartic potential induces a convex correction to the nearly uniform charge distribution in the center of the perfect parabolic QWW. For $A_4 < 0$, the effect of the nonparabolicity on the charge-density profile is more dramatic as for $A_4 > 0$. It is seen that with increasing magnitude of the nonparabolicity, the charges become concentrated more and more at the edges of the well for higher electron density, i.e. if more subbands are occupied. Figure 5 shows the different initial potentials (bare potentials) and the corresponding self-consistent potentials for two different electron densities.

III. DENSITY RESPONSE OF A Q1DEG

In this chapter, we calculate the response of a Q1DEG to an external potential on a quantum-mechanical level

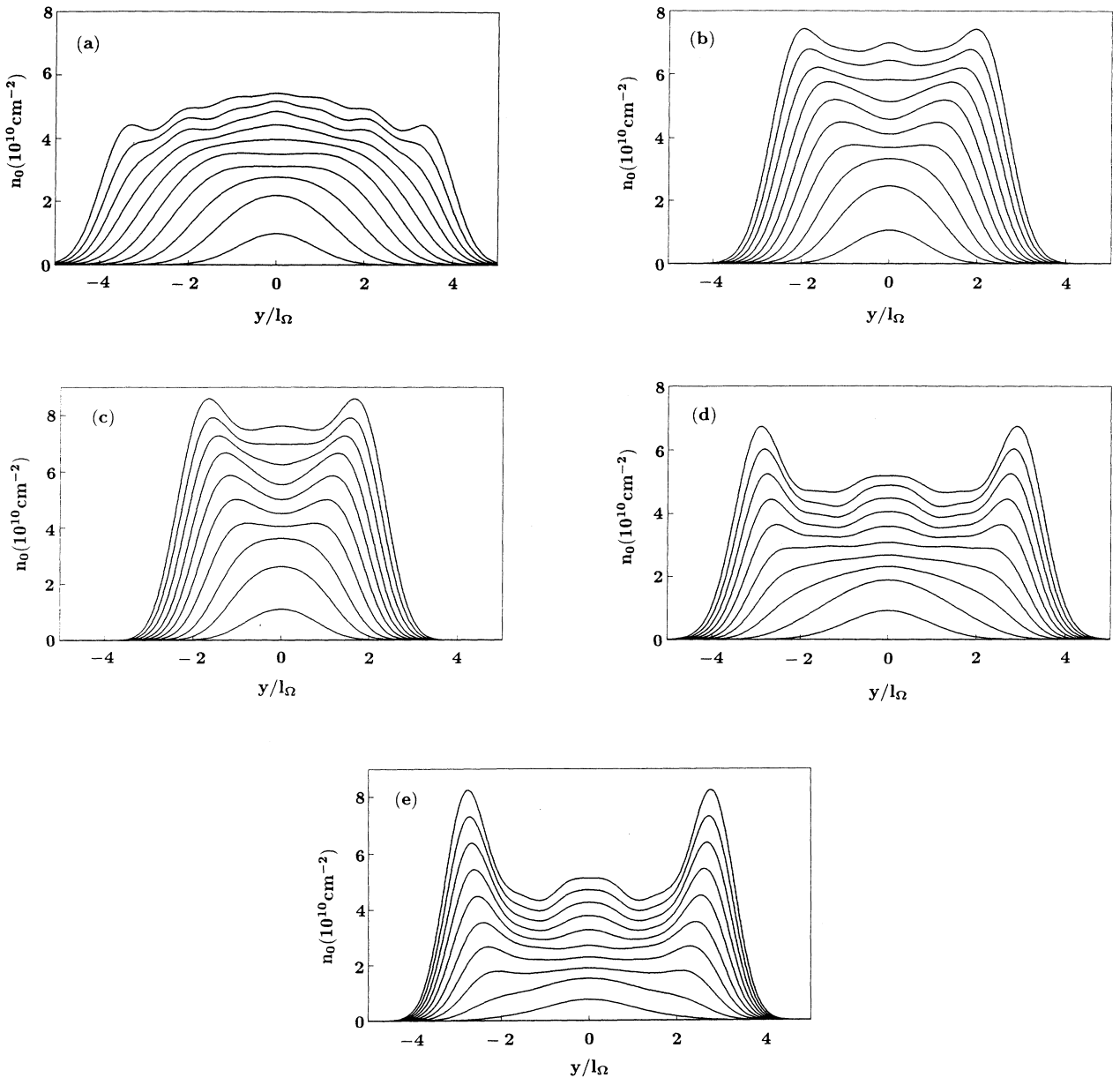

FIG. 4. Charge density profiles in different QWW's: (a) $A_4 = A_6 = 0$; (b) $A_4 = 0.05\,\hbar\Omega/l_\Omega^4, A_6 = 0$; (c) $A_4 = 0.1\,\hbar\Omega/l_\Omega^4, A_6 = 0$; (d) $A_4 = -0.05\,\hbar\Omega/l_\Omega^4$, $A_6 = 0.003\,33\,\hbar\Omega/l_\Omega^6$; (e) $A_4 = -0.1\,\hbar\Omega/l_\Omega^4$, $A_6 = 0.0075\,\hbar\Omega/l_\Omega^6$. The heavy solid lines denote the profiles at different densities: the lowest curves correspond to $n_{1\mathrm{DEG}} = 0.5 \times 10^5\ \mathrm{cm}^{-1}$ and the higher curves are calculated with $\Delta n_{1\mathrm{DEG}} = 1 \times 10^5\ \mathrm{cm}^{-1}$.

within the RPA, using the *self-consistent field* (SCF) method. The single-particle Hamiltonian of the electrons of the Q1DEG in the presence of the perturbation is written as $H = H_0 + H_1$, where H_0 is the unperturbed Hamiltonian of a single electron in the QWW, which satisfies the Schrödinger equation $H_0|L,k_x\rangle = \mathcal{E}_L|L,k_x\rangle$ and $H_1 = V^{\rm sc}(\mathbf{x},t)$ is the self-consistent potential. Writing the statistical operator ρ_G of the system as $\rho_G = \rho_G^{(0)} + \rho_G^{(1)}$, where $\rho_G^{(0)}$ is the statistical operator of the unperturbed system, and $\rho_G^{(1)}$ is the correction to the statistical operator to the first order in the perturbation, it follows from the single-particle von Neumann equation,

$$\langle L,k_x|\rho_G^{(1)}|L',k_x'\rangle = \frac{n_F(\mathcal{E}_{L'}(k_x')) - n_F(\mathcal{E}_L(k_x))}{\hbar(\omega+i\delta) + \mathcal{E}_{L'}(k_x') - \mathcal{E}_L(k_x)} \times \langle L,k_x|V^{\rm sc}(\mathbf{x},\omega)|L',k_x'\rangle \,, \tag{21}$$

where $\rho_G^{(0)}|L,k_x\rangle = n_F(\mathcal{E}_L(k_x))|L,k_x\rangle$ is used with $n_F(\mathcal{E}_L(k_x)) = \Theta[E_F - \mathcal{E}_L(k_x)]$, the Fermi distribution function at $T = 0$ K. The total electron number density $n = n_0 + n_{\rm ind}$ of the Q1DEG is a sum of the equilibrium ground-state electron number density n_0 and the induced electron number density $n_{\rm ind}(\mathbf{x},\omega) = {\rm Tr}\{\rho_G^{(1)}\delta(\mathbf{x}-\mathbf{x}_e)\}$ caused by the perturbation. The evaluation of the trace (Tr) gives

$$n_{\rm ind}(\mathbf{x},\omega) = \int d^3x' P^{(1)}(\mathbf{x},\mathbf{x}'|\omega) V^{\rm sc}(\mathbf{x}',\omega) \,. \tag{22}$$

In this equation, $P^{(1)}(\mathbf{x},\mathbf{x}'|\omega)$ is the *irreducible* RPA *polarization function* of the Q1DEG,

$$P^{(1)}(\mathbf{x},\mathbf{x}'|\omega) = \frac{1}{L_x}\sum_{q_x} e^{iq_x(x-x')}\, P^{(1)}(q_x;\mathbf{x}_\perp,\mathbf{x}_\perp'|\omega) \,, \tag{23}$$

$$P^{(1)}(q_x;\mathbf{x}_\perp,\mathbf{x}_\perp'|\omega) = \sum_{L,L'} P^{(1)}_{LL'}(q_x,\omega)\, \eta_{LL'}(\mathbf{x}_\perp)\eta^*_{LL'}(\mathbf{x}_\perp') \,, \tag{24}$$

with the RPA *matrix polarization function*

$$P^{(1)}_{LL'}(q_x,\omega) = \frac{2}{L_x}\sum_{k_x} \frac{n_F(\mathcal{E}_{L'}(k_x)) - n_F[\mathcal{E}_L(k_x+q_x)]}{\hbar(\omega+i\delta) + \mathcal{E}_{L'}(k_x) - \mathcal{E}_L(k_x+q_x)} \,, \tag{25}$$

$$\eta_{LL'}(\mathbf{x}_\perp) = \xi_L(y)\,\xi^*_{L'}(y)\,\delta(z), \tag{26}$$

and $\mathbf{x}_\perp = (0,y,z)$. Within the RPA and at $T = 0$ K the real part of the matrix polarization function is[8]

$$\begin{aligned}{\rm Re}\, P^{(1)}_{LL'}(q_x,\omega) &= -\frac{m_e}{\pi\hbar^2 q_x}\left\{ \ln\left| \frac{k_F^{(L')} + \frac{q_x}{2} - \frac{m_e}{\hbar q_x}(\omega - \Omega_{LL'})}{k_F^{(L')} - \frac{q_x}{2} + \frac{m_e}{\hbar q_x}(\omega - \Omega_{LL'})} \right| \right. \\ &\left. + \ln\left| \frac{k_F^{(L)} + \frac{q_x}{2} + \frac{m_e}{\hbar q_x}(\omega - \Omega_{LL'})}{k_F^{(L)} - \frac{q_x}{2} - \frac{m_e}{\hbar q_x}(\omega - \Omega_{LL'})} \right| \right\} \,, \end{aligned} \tag{27}$$

where $\Omega_{LL'} = (\mathcal{E}_L - \mathcal{E}_{L'})/\hbar$ is the subband separation frequency, and the imaginary part reads

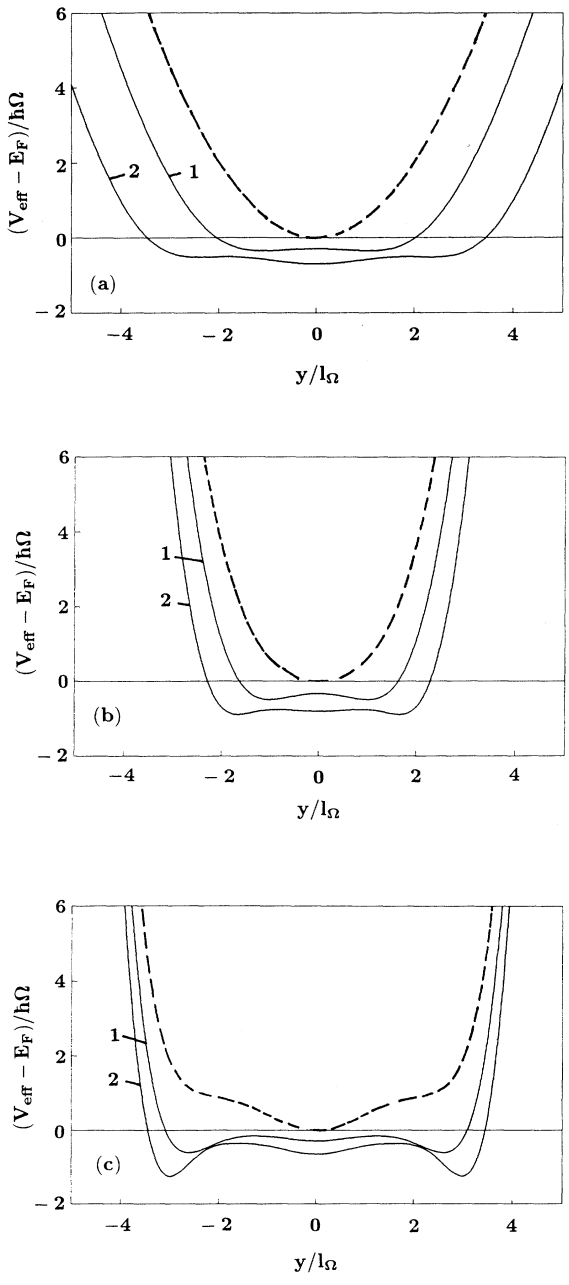

FIG. 5. Bare potential $V_0(y)$ (dashed line) and effective potential $V_{\rm eff}(y)$ (solid line) for two different electron densities (1) $n_{\rm 1DEG} = 1.5\times10^5$ cm^{-1} and (2) $n_{\rm 1DEG} = 4.5\times10^5$ cm^{-1} of different QWW's: (a) $A_4 = A_6 = 0$; (b) $A_4 = 0.1\,\hbar\Omega/l_\Omega^4$, $A_6 = 0$; and (c) $A_4 = -0.1\,\hbar\Omega/l_\Omega^4$, $A_6 = 0.0075\,\hbar\Omega/l_\Omega^6$.

$$\mathrm{Im}\, P^{(1)}_{LL'}(q_x,\omega) = -\frac{m_e}{\hbar^2|q_x|}\left\{\Theta\left[k_F^{(L')}+\frac{q_x}{2}-\frac{m_e}{\hbar q_x}(\omega-\Omega_{LL'})\right]\Theta\left[k_F^{(L')}-\frac{q_x}{2}+\frac{m_e}{\hbar q_x}(\omega-\Omega_{LL'})\right]\right.$$
$$\left.-\Theta\left[k_F^{(L)}+\frac{q_x}{2}+\frac{m_e}{\hbar q_x}(\omega-\Omega_{LL'})\right]\Theta\left[k_F^{(L)}-\frac{q_x}{2}-\frac{m_e}{\hbar q_x}(\omega-\Omega_{LL'})\right]\right\}. \quad (28)$$

The self-consistent potential $V^{\mathrm{sc}}(\mathbf{x},\omega)$ is a sum of the external potential $V^{\mathrm{ext}}(\mathbf{x},\omega)$ and the induced potential $V^{\mathrm{ind}}(\mathbf{x},\omega)$, which results from the induced density: $V^{\mathrm{sc}}(\mathbf{x},\omega) = V^{\mathrm{ext}}(\mathbf{x},\omega) + V^{\mathrm{ind}}(\mathbf{x},\omega)$. In the RPA and neglecting retardation effects, the induced potential is related to the induced density by Poisson's equation,

$$\nabla\cdot[\varepsilon_s(\mathbf{x})\,\nabla V^{\mathrm{ind}}(\mathbf{x},\omega)] = -\frac{e^2}{\varepsilon_0}\,n_{\mathrm{ind}}(\mathbf{x},\omega)\,. \quad (29)$$

The use of $\varepsilon_s(\mathbf{x})$ in Eq. (29) takes into account the static screening of the optical phonons, which have frequencies usual larger than those of the collective excitations of the Q1DEG. The case that the frequencies of both excitations are in the same order makes it necessary to include the contribution of the optical phonons to the self-consistent potential dynamically, as developed in Ref. 8. Further, the frequencies of the acoustic phonons are much smaller than those of the collective excitations of the Q1DEG and hence, can be neglected. On the grounds of this typical situation, we can use the ε_s *approximation* for the screening of the dielectric background.

Neglecting image effects and using the translational symmetry of the QWW along the x axis by one-dimensional Fourier series,

$$V^{\mathrm{ind}}(\mathbf{x},\omega) = \frac{1}{L_x}\sum_{q_x} e^{iq_x x}V^{\mathrm{ind}}(q_x;\mathbf{x}_\perp|\omega) \quad (30)$$

and

$$V^{\mathrm{ind}}(q_x;\mathbf{x}_\perp|\omega) = \int dx\; e^{-iq_x x}\; V^{\mathrm{ind}}(\mathbf{x},\omega)\,, \quad (31)$$

the self-consistent potential is given by

$$V^{\mathrm{sc}}(q_x;\mathbf{x}_\perp|\omega) = V^{\mathrm{ext}}(q_x;\mathbf{x}_\perp) + \frac{e^2}{2\pi\varepsilon_0\varepsilon_s}\int d^2x'_\perp \times\int d^2x''_\perp\; K_0[|q_x(\mathbf{x}_\perp-\mathbf{x}'_\perp)|] \times P^{(1)}(q_x;\mathbf{x}'_\perp,\mathbf{x}''_\perp|\omega)\; V^{\mathrm{sc}}(q_x;\mathbf{x}''_\perp|\omega)\,, \quad (32)$$

where K_0 is the modified Bessel function of zeroth order. Performing matrix elements of this equation, using Eq. (24) and assuming that the collective excitations of the Q1DEG exist under the condition that $V^{\mathrm{sc}} \neq 0$ while $V^{\mathrm{ext}} = 0$, the existence condition for the collective excitations reads

$$\sum_{L,L'}[\delta_{L_1L}\delta_{L_2L'} - V^s_{L_1L_2L'L}(q_x)\,P^{(1)}_{LL'}(q_x,\omega)]\;V^{\mathrm{sc}}_{LL'}(q_x,\omega) = 0\,, \quad (33)$$

where

$$V^s_{L_1L_2L_3L_4}(q_x) = \frac{e^2}{2\pi\varepsilon_0\varepsilon_s}\int_{-\infty}^{\infty}dy\int_{-\infty}^{\infty}dy'\;\xi^*_{L_1}(y)\;\xi_{L_2}(y) \times K_0[|q_x(y-y^1)|]\;\xi^*_{L_3}(y')\;\xi_{L_4}(y'), \quad (34)$$

and

$$V^{\mathrm{sc}}_{LL'}(q_x,\omega) = \int_{-\infty}^{\infty}dy\;\xi^*_L(y)\;V^{\mathrm{sc}}(q_x;y|\omega)\;\xi_{L'}(y)\,. \quad (35)$$

If the confining potential is mirror symmetric, the effective potential has the same spatial symmetry. In this case, i.e., if $V_{\mathrm{eff}}(y) = V_{\mathrm{eff}}(-y)$, the parity of the single-particle states $\xi_L(y)$ results in $V^s_{L_1L_2L_3L_4}(q_x) = 0$ if $(L_1+L_2+L_3+L_4)$ is an odd number. Further, for bound electrons under consideration the envelope wave functions $\xi_L(y)$ are real and hence, we have the symmetries: $V^s_{L_1L_2L_3L_4} = V^s_{L_2L_1L_3L_4} = V^s_{L_1L_2L_4L_3} = V^s_{L_3L_4L_1L_2}$ and $V^{\mathrm{sc}}_{LL'} = V^{\mathrm{sc}}_{L'L}$. What follows is that Eq. (33) splits into two separate systems of equations:

$$\sum_{L=0}^{M-1}\sum_{n=0}^{\left[\frac{N-1}{2}\right]}[\delta_{L_1,L}\delta_{L_2,L+2n} - V^s_{L_1L_2L+2nL}(q_x)\chi^{(1)}_{LL+2n}(q_x,\omega)]\;V^{\mathrm{sc}}_{LL+2n}(q_x,\omega) = 0 \quad (36)$$

and

$$\sum_{L=0}^{M-1}\sum_{n=0}^{\left[\frac{N}{2}-1\right]}[\delta_{L_1,L}\delta_{L_2,L+(2n+1)} - V^s_{L_1L_2L+(2n+1)L}(q_x)\chi^{(1)}_{LL+(2n+1)}(q_x,\omega)] \times V^{\mathrm{sc}}_{LL+(2n+1)}(q_x,\omega) = 0\,, \quad (37)$$

where $[x]$ denotes the integral part of x. In Eqs. (36) and (37), we have assumed that we restrict the consideration on N subbands, from which $M \leq N$ subbands are occupied: $L_i = 0,1,2,\ldots,N-1$. The restriction on a small number of subbands $L, L' = 0,\ldots,N-1$ is possible because the matrix polarization function has the properties $P^{(1)}_{LL'}(q_x,\omega) \to 0$ for large $|L-L'|$, $P^{(1)}_{LL'}(q_x,\omega) = 0$ if $E_F \leq \mathcal{E}_L, \mathcal{E}_{L'}$ and usual only a few subbands are occupied. In Eqs. (36) and (37), we have defined

$$\chi^{(1)}_{LL'}(q_x,\omega) = \frac{P^{(1)}_{LL'}(q_x,\omega)+P^{(1)}_{L'L}(q_x,\omega)}{1+\delta_{LL'}}\,. \quad (38)$$

Equation (36) describes collective electron transitions

between states with the same parity, whereas Eq. (37) describes such transitions between states with opposite parity. The corresponding secular equations,

$$\det[\delta_{L_1 L}\delta_{L_2 L+2n} - V^s_{L_1 L_2 L+2n L}(q_x)\chi^{(1)}_{LL+2n}(q_x,\omega)] = 0 \ , \tag{39}$$

with determinants of order $M \times [(N+1)/2]$ and

$$\det[\delta_{L_1 L}\delta_{L_2 L+(2n+1)} - V^s_{L_1 L_2 L+(2n+1)L}(q_x)\chi^{(1)}_{LL+(2n+1)}(q_x,\omega)] = 0 \ , \tag{40}$$

with determinants of order $M \times [N/2]$, are the *dispersion relations* of the *symmetric* Q1D plasmons (even parity modes) and the *antisymmetric* Q1D plasmons (odd parity modes), respectively, under the condition that $\mathrm{Im}\chi^{(1)}_{LL'}(q_x,\omega) = 0$. The *symmetric modes* are connected with all electron transitions between states with the same parity and the *antisymmetric modes* are connected with all electron transitions between states with opposite parity. We remark that all the transitions between states of the same parity are coupled but independent from that between states of opposite parity. Only in a *diagonal approximation*, i.e., by retaining only the elements of $V^s_{L_1 L_2 L_3 L_4}(q_x)\chi^{(1)}_{L_4 L_3}(q_x,\omega) = \delta_{L_1 L_3}\delta_{L_2 L_4} V^s_{L_1 L_2 L_1 L_2}(q_x)\chi^{(1)}_{L_2 L_1}(q_x\omega)$, do all the intersubband transitions become independent and to each transition exists one Q1D plasmon. Then a plasmon is called an $(L-L)$ *intrasubband plasmon* if the collective electron transition is within the subband $\mathcal{E}_L$, and it is called an $(L'-L)$ *intersubband plasmon* if the collective intersubband transition is between the subbands $\mathcal{E}_L \leftrightarrow \mathcal{E}_{L'}$. With coupling between the different transitions, the Q1D plasmons become *hybrid* (or *mixed*) modes with different branches of dispersion curves. The regions, where $\mathrm{Im}\chi^{(1)}_{LL'}(q_x,\omega) \neq 0$ define the regions in the $\omega - q_x$ plane for the existence of the *single-particle excitations* (SPE's). Within the RPA, the SPE's are not coupled because noninteracting electrons are considered and hence, represent independent single-particle transitions: (i) within one subband, which are called *single-particle intrasubband excitations*, and (ii) between different subbands, which are called *single-particle intersubband excitations*. The SPE's have a continuous spectrum with the boundaries,

$$\omega^{LL'}_{1,2} = \left| \pm \frac{\hbar k_F^{(L')} q_x}{m_e} + \frac{\hbar q_x^2}{2m_e} + \Omega_{LL'} \right| \tag{41}$$

and

$$\omega^{LL'}_{3,4} = \left| \pm \frac{\hbar k_F^{(L)} q_x}{m_e} - \frac{\hbar q_x^2}{2m_e} + \Omega_{LL'} \right| \ . \tag{42}$$

To solve the dispersion relations, Eqs. (39) and (40), in the self-consistent procedure, we use the renormalized subband energies $\mathcal{E}_L$ and wave functions $\xi_L(y)$ from Eq. (15). Then the Coulomb matrix element reads

$$V^s_{L_1 L_2 L_3 L_4}(q_x) = \frac{e^2}{2\pi\varepsilon_0\varepsilon_s} \sum_{L_1' L_2' L_3' L_4'} C_{L_1 L_1'}\, C_{L_2 L_2'}\, C_{L_3 L_3'} \times C_{L_4 L_4'}\, f^C_{L_1' L_2' L_3' L_4'}(q_x) \ , \tag{43}$$

with

$$f^C_{L_1 L_2 L_3 L_4}(q_x) = (-1)^{L_1+L_2}\delta_{L_1+L_2+L_3+L_4,2n}\sqrt{L_1!L_2!L_3!L_4!}\, e^a \sum_{m_2=0}^{L_2}\sum_{m_4=0}^{L_4}\sum_{\nu=0}^{\lambda}(-1)^\nu \times \frac{a^\lambda C^\lambda_\nu (2\lambda-1)!! K_\nu(a)}{m_2! m_4! (L_2-m_2)!(L_4-m_4)!(L_1-L_2+m_2)!(L_3-L_4+m_4)!(\lambda-\nu)!} \ , \tag{44}$$

where $n = 0,1,2,\ldots$, $a = (l_\Omega q_x/2)^2$, $\lambda = m_2+m_4+(L_1-L_2+L_3-L_4)/2$, $(2\lambda-1)!! = 1\cdot 3\cdot\ldots\cdot(2\lambda-1)$, and

$$C^\lambda_\nu = \begin{cases} \frac{1}{(\lambda+1)\cdots(\lambda+\nu)} & \text{if } \nu \neq 0 \\ \frac{1}{2} & \text{if } \nu = 0 \ . \end{cases} \tag{45}$$

Equation (44) is valid for $L_1 \geq L_2$ and $L_3 \geq L_4$. The opposite case follows from the symmetry relation $f^C_{L_1 L_2 L_3 L_4}(q_x) = f^C_{L_2 L_1 L_3 L_4}(q_x)$. The coefficients $C_{LL'}$ are the expansion coefficients of the wave function in Eq. (12).

IV. COLLECTIVE EXCITATIONS: SELF-CONSISTENT CALCULATION OF Q1D PLASMONS

A. Bare perfect parabolic potential

In this chapter, we represent numerical results of the self-consistent calculation of the dispersion relation of Q1D plasmons in parabolic QWW's. The self-consistent full RPA dispersion relations of the Q1D plasmons (heavy solid lines) in dependence on the wave vector are plotted for a perfect parabolic QWW in Fig. 6 for the symmetric modes and in Fig. 7 for the antisymmetric modes. In addition, the shaded areas are the SPE continua with the boundaries given by Eqs. (41) and (42). In these

calculations, we have assumed for the number of subbands $L = 0, 1, \ldots, N-1$ in the calculation: $N = M+3$, i.e., we use a $(M+3)$-*subband model*, where M is the number of occupied subbands. The case of one occupied subband is plotted in Figs. 6(a) and 7(a) and Figs. 6(b) and 7(b) show the Q1D plasmon dispersion curves for two occupied subbands. In the case of one occupied subband [Fig. 6(a)], there are two symmetric plasmon modes, denoted by ω_p^{00} and ω_p^{20}, both accompanied with the collective electron transitions $0 \leftrightarrow 0$ and $0 \leftrightarrow 2$. The branch ω_p^{00} is accompanied mostly with collective electron transitions within the lowest subband $0 \leftrightarrow 0$, whereas ω_p^{20} is dominated by $0 \leftrightarrow 2$ transitions. Hence, one should identify ω_p^{00} as an intrasubband (-like) plasmon and ω_p^{20} as an intersubband (-like) plasmon. If two subbands are occupied, the Q1D plasmons are the mixed $(0-0)$-$(1-1)$-$(2-0)$-$(3-1)$ plasmons with four branches of dispersion curves. It is seen that the branches denoted by ω_p^{11} and ω_p^{31}, which are dominated by the collective electron transitions $1 \leftrightarrow 1$ and $1 \leftrightarrow 3$, respectively, appear in this case. It was shown[14] that the electron densities induced in subbands $\mathcal{E}_0(k_x)$ and $\mathcal{E}_1(k_x)$ oscillate *in phase* if branch ω_p^{00} is excited, but in *antiphase* if the branch ω_p^{11} is excited, i.e., ω_p^{00} behaves like an *optical* and ω_p^{11} like an *acoustic* plasmon. The antisymmetric modes of a perfect parabolic QWW with one occupied subband are the mixed $(1-0)$-$(3-0)$ plasmons with two branches, ω_p^{10} and ω_p^{30}, of the dispersion relation. It becomes obvious that the branch ω_p^{10}, which

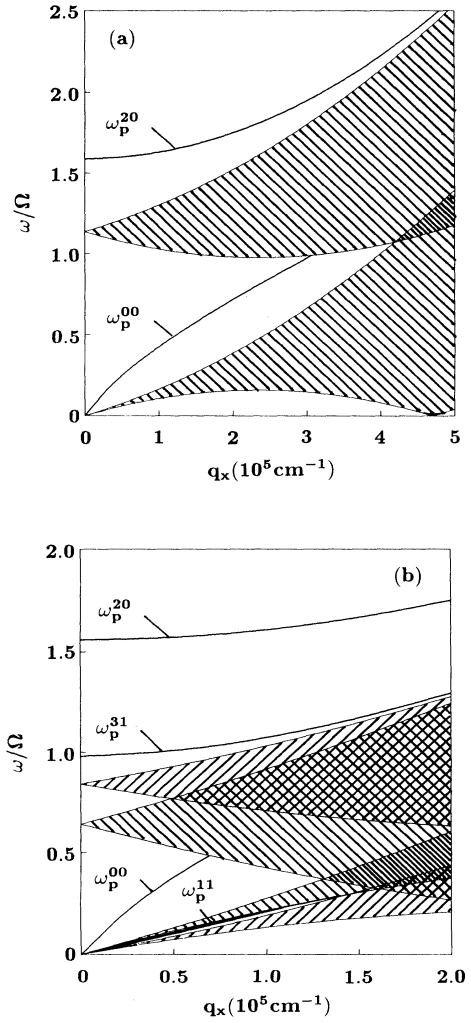

FIG. 6. Dispersion relation of the symmetric plasmons calculated self-consistently in RPA in dependence on the wave vector component q_x for a bare perfect parabolic potential: (a) one subband is occupied ($n_{1DEG} = 1.5 \times 10^5$ cm^{-1}), (b) two subbands are occupied ($n_{1DEG} = 4.5 \times 10^5$ cm^{-1}).

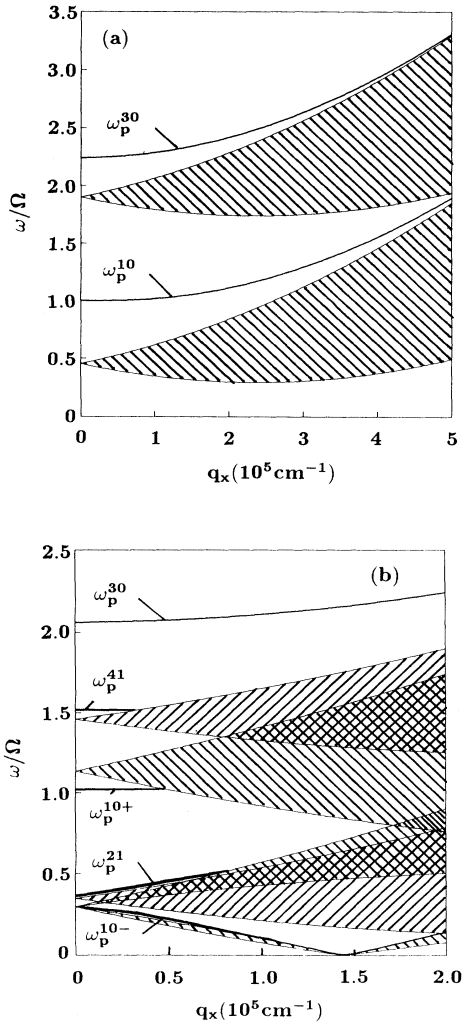

FIG. 7. Dispersion relation of the antisymmetric intersubband plasmons calculated self-consistently in RPA in dependence on the wave vector component q_x for a bare perfect parabolic potential: (a) one subband is occupied ($n_{1DEG} = 1.5 \times 10^5$ cm^{-1}), (b) two subbands are occupied ($n_{1DEG} = 4.5 \times 10^5$ cm^{-1}).

is mostly accompanied by the collective electron transition $0 \leftrightarrow 1$, has for $q_x = 0$ a frequency identical to the bare harmonic oscillator frequency: $\omega_p^{10}(q_x = 0) = \Omega$. Hence, this mode becomes for vanishing wave vector the so-called *fundamental or Kohn's mode*, i.e., is accompanied only by the center-of-mass motion of the confined electrons. The manifestation of Kohn's theorem in the spectrum of Q1D plasmons is that the renormalization of the subband separation frequency from Ω of the perfect bare potential to $\Omega_{10} = (\mathcal{E}_1 - \mathcal{E}_0)/\hbar$ of the effective potential is exactly compensated by the depolarization shift $\Delta_p^{10} = \omega_p^{10}(q_x = 0) - \Omega_{10}$, i.e., $\Omega = \Omega_{10} + \Delta_p^{10}$ is valid with a *finite* depolarization shift. This corresponds with our earlier result,[9] where it was shown analytically by first-order perturbation theory that the Hartree renormalization of the subband energy spacing is compensated by the Hartree screening of the collective intersubband resonance. In the case of two occupied subbands, it is seen that the hybrid modes ω_p^{21} and ω_p^{41} occur in addition to the case of one occupied subband and the mode ω_p^{10} splits into *two branches*: ω_p^{10+} and ω_p^{10-}. The lower-frequency mode occurs inside the gap of the single-particle $(1-0)$ intersubband continuum.[8] It was shown recently[14] that the electron densities induced in subbands $\mathcal{E}_0(k_x)$ and $\mathcal{E}_1(k_x)$ oscillate in antiphase if the branches $\omega_p^{10\pm}$ are excited, i.e., $\omega_p^{10\pm}$ behave like acoustic plasmons. It is seen that for $q_x = 0$, the branch ω_p^{10+} has the frequency Ω, i.e., is independent from the number of electrons in the QWW.

In the FIR transmission experiments with perpendicularly incident light, only the intersubband resonance (dimensional resonance) $\omega_p^{10}(q_x = 0) = \Omega$ is measured in difference to the occurrence of many branches of collective intersubband transitions. The calculated modes are the independent *free* oscillating states of the QWW. If the applied light couples with the modes, the corresponding positions of the minima in the FIR spectrum give the frequencies of the modes. But only those modes which have a nonvanishing induced electric dipole moment can couple with light. In the case of a bare perfect parabolic potential and vanishing wave vector component $q_x = 0$, only the collective intersubband resonance $\omega_p^{10} = \Omega$ has a nonvanishing induced electric dipole moment and hence, is observable in a FIR experiment. All the other modes, which are accompanied with relative electron motions, cannot be detected in this case with FIR spectroscopy.

Figure 8 shows the dispersion curves of the antisymmetric modes $\omega_p^{L+1,L}$ of a QWW with a bare perfect parabolic potential in dependence on the electron density in the wire. It is seen that for $q_x = 0$, the branch ω_p^{10} is pinned at the bare harmonic oscillator frequency. The small deviations of ω_p^{10} from Ω are due to the approximations used. Notice, that for $q_x = 0$ the SPE continua degenerate to the lines $\Omega_{LL'}$. The generalized Kohn's theorem is an exact result, but, here, we use the Hartree approximation for the ground state and the RPA for the response and further neglect higher-frequency modes than $\omega_p^{L+5,L}$. It is seen that the modes ω_p^{21} and ω_p^{32} start at the onset of the occupation of the subbands $\mathcal{E}_1(k_x)$ and $\mathcal{E}_2(k_x)$, respectively, and have a very small depolarization shift. Hence, for large electron densities, we have only one mode with a large depolarization shift, ω_p^{10}, but $M-1$ modes forming a band of modes which have only small depolarization shifts, i.e., the band is placed near the corresponding single-particle transition frequencies. This physical property of the collective intersubband resonances in QWW's with bare perfect parabolic potentials is qualitatively very similar to the case of a QWW with an *effective* perfect parabolic potential $V_{\text{eff}}(y) = m_e\Omega^2 y^2/2$.[4,9] For a finite wave vector component q_x, it is seen that for electron densities where the second subband becomes occupied, the gap region in the single-particle $(1-0)$ continuum is opened in which the mode ω_p^{10-} exists and with the occupation of the third subband, the gap region in the single-particle $(2-1)$ continuum is opened, having the mode ω_p^{21-} inside. For $q_x \neq 0$, Kohn's theorem becomes invalid and this is manifested in Fig. 8(b) by a frequency of ω_p^{10+} higher than Ω. Additionally, the frequency of ω_p^{10+} slightly depends on the electron density. With increasing wave vector, this dependence increases in magnitude. Figure 9 shows the dispersion curves of the symmetric modes $\omega_p^{L+2,L}$ of a QWW with a bare perfect parabolic potential in dependence on the electron density in the wire. It is seen that already for $q_x = 0$ the frequencies of all modes depend

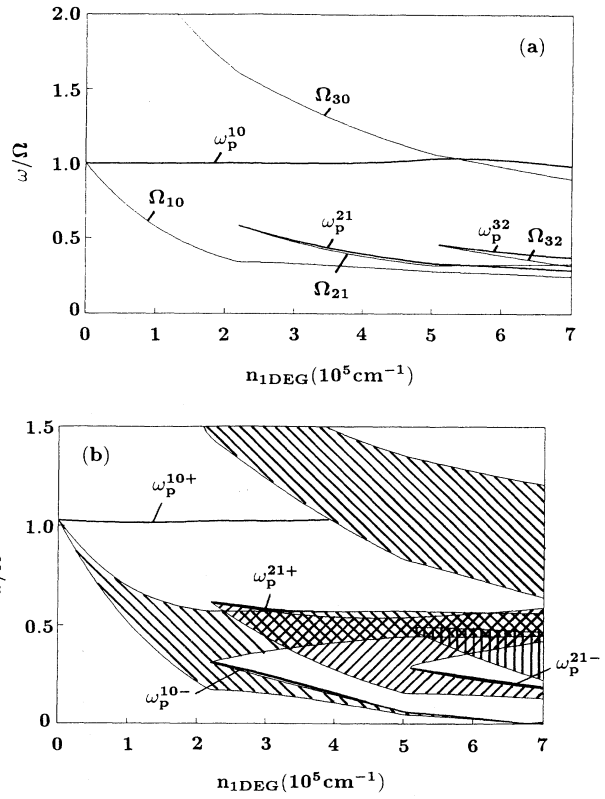

FIG. 8. Dispersion relation of the antisymmetric intersubband plasmons $\omega_p^{L+1,L}$ in dependence on the electron density in the QWW with a bare perfect parabolic potential for (a) $q_x = 0$ and (b) $q_x = 1 \times 10^5$ cm^{-1}. For $q_x = 0$, the continua of the SPE degenerate to the lines $\Omega_{L+1,L}$.

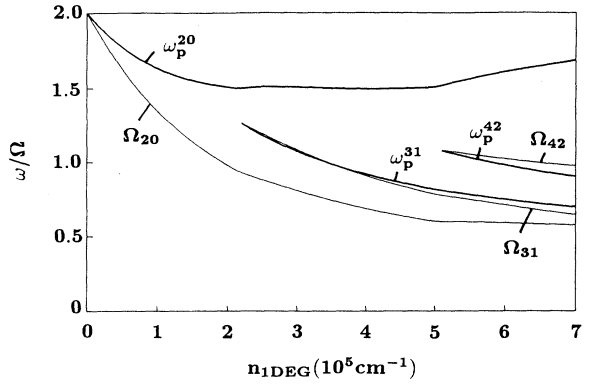

FIG. 9. Dispersion relation of the symmetric intersubband plasmons $\omega_p^{L+2,L}$ in dependence on the electron density in the QWW with a bare perfect parabolic potential for $q_x = 0$. For $q_x = 0$, the continua of the SPE degenerate to the lines $\Omega_{L+2,L}$.

on the electron density. This underlines the very special feature of the mode $\omega_p^{10}(q_x = 0) = \Omega$ in the case of bare perfect parabolic potentials.

If one performs FIR transmission experiments on QWW's with a grating coupler directed orthogonal to the wire axis on top of the sample, it is possible to excite the plasmons with $q_x = \frac{2\pi}{d}n; n = 0, \pm 1, \pm 2, \ldots$ (d denotes the period of the grating). For a bare parabolic potential, one observes in the case $q_x \neq 0$ all the antisymmetric modes because these modes become dipole active.

B. Bare nonparabolic potential

Let us examine the nonparabolicity effects of the bare potential on the dispersion curves of the Q1D plasmons. In Fig. 10, the dispersion curves of the antisymmetric modes $\omega_p^{L+1,L}$ of a QWW are plotted for $q_x = 0$ in dependence on the electron density for different bare nonparabolic potentials. It is seen from all figures that the nonparabolicity causes a deviation of the branch ω_p^{10}

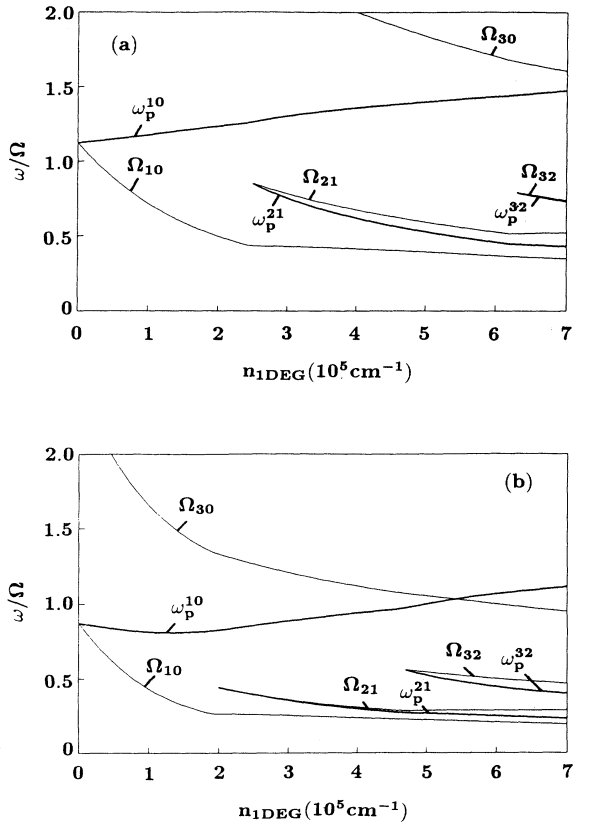

FIG. 10. Dispersion relation of the antisymmetric intersubband plasmons $\omega_p^{L+1,L}$ at $q_x = 0$ in dependence on the electron density for different imperfections of the bare parabolic confining potential: (a) $A_4 = 0.05\,\hbar\Omega/l_\Omega^4$, $A_6 = 0$ and (b) $A_4 = -0.05\,\hbar\Omega/l_\Omega^4$, $A_6 = 0.003\,33\,\hbar\Omega/l_\Omega^6$. For $q_x = 0$, the continua of the SPE degenerate to the lines $\Omega_{L+1,L}$.

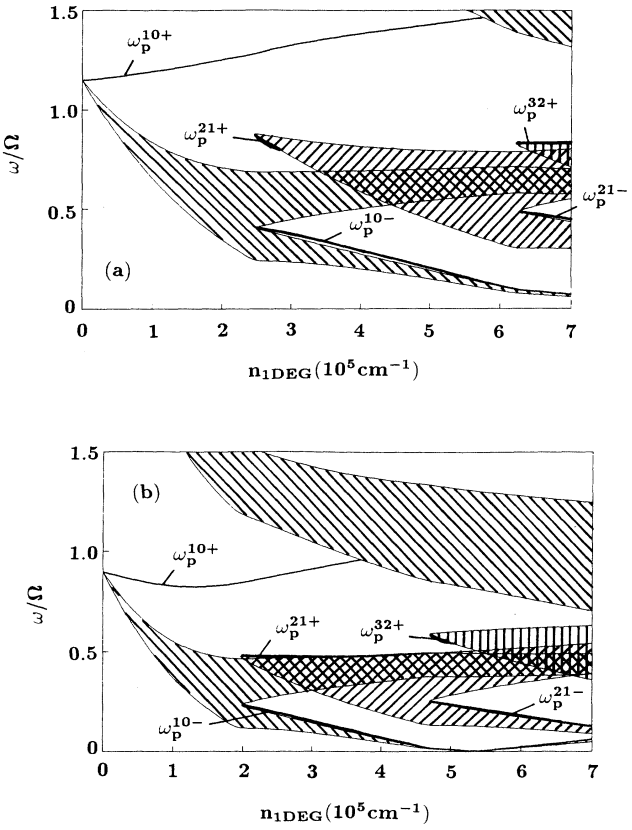

FIG. 11. Dispersion relation of the antisymmetric intersubband plasmons $\omega_p^{L+1,L}$ at $q_x = 1 \times 10^5$ cm^{-1} in dependence on the electron density for different imperfections of the bare parabolic confining potential: (a) $A_4 = 0.05\,\hbar\Omega/l_\Omega^4$, $A_6 = 0$ and (b) $A_4 = -0.05\,\hbar\Omega/l_\Omega^4$, $A_6 = 0.003\,33\,\hbar\Omega/l_\Omega^6$.

from Ω and results, in general, in an increasing magnitude of ω_p^{10} with increasing electron density. In the case that the quartic term is positive ($A_4 > 0$), the fundamental mode ω_p^{10} is shifted above Ω and increases monotonously with $n_{1\mathrm{DEG}}$. The branches ω_p^{21} and ω_p^{32} are also shifted to higher frequencies in comparison to the perfect parabolic case and decrease more rapidly with $n_{1\mathrm{DEG}}$ as for $A_4 = A_6 = 0$. But in this case, the branches ω_p^{21} and ω_p^{32} appear with a *negative* depolarization shift, i.e., an "antiscreening" of the corresponding transitions takes place. For $A_4 < 0$, the modes ω_p^{10} and ω_p^{21} are shifted to smaller frequencies at their low-density start point, but ω_p^{32} is shifted to higher frequencies in comparison to the case of a bare perfect parabolic potential. The modes ω_p^{21} and ω_p^{32} again have a negative depolarization shift. The curve ω_p^{10} in dependence on $n_{1\mathrm{DEG}}$ shows a broad minimum slightly below the critical density, where

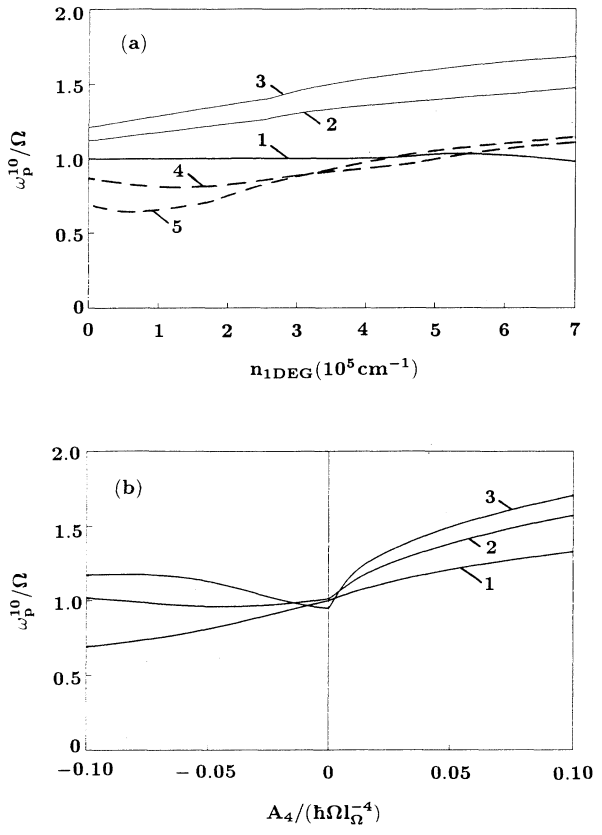

FIG. 12. Frequency of the mode ω_p^{10} (intersubband resonance) at $q_x = 0$ in dependence on (a) the electron density in the QWW with different confining potentials; (1) bare perfect parabolic potential (heavy solid line), $A_4 = A_6 = 0$ and bare nonparabolic potentials, $A_4 > 0, A_6 = 0$ (thin solid lines); (2) $A_4 = 0.05\,\hbar\Omega/l_\Omega^4$; (3) $A_4 = 0.1\,\hbar\Omega/l_\Omega^4$ and $A_4 < 0, A_6 > 0$ (dashed lines); (4) $A_4 = -0.05\,\hbar\Omega/l_\Omega^4$, $A_6 = 0.003\,33\,\hbar\Omega/l_\Omega^6$; (5) $A_4 = -0.1\,\hbar\Omega/l_\Omega^4$, $A_6 = 0.0075\,\hbar\Omega/l_\Omega^6$; and (b) in dependence on the nonparabolicity parameter A_4 (A_6 see Fig. 3) for three different densities (see Fig. 3).

the second subband becomes occupied. Figure 11 shows the corresponding dispersion curves for $q_x \neq 0$. For the mode ω_p^{10}, nearly the same happens as for $q_x = 0$. More dramatic is the effect of imperfections of the parabolic confining potential on the modes $\omega_p^{21\pm}$ and $\omega_p^{32\pm}$. Besides of appreciable frequency shifts, the existence regions of these modes become shifted drastically. This becomes obvious from Figs. 8(b), 11(a), and 11(b), where the mode ω_p^{21+} exists for $A_4 > 0$ only in a very small density range. But this range increases with increasing A_4. To see the influence of the nonparabolicity on the fundamental mode ω_p^{10} more explicitely, we have plotted its dependence on the density for the different potentials and its dependence on the nonparabolicity parameter in Fig. 12. Figure 12(a) shows very clear the deviations from the special situation, where Kohn's theorem is valid. In general, it is seen that nonparabolic confining potentials influence the collective intersubband transition ω_p^{10} in such a manner that its frequency increases with increasing densities in the general tendency. From Fig. 12(b) it becomes obvious that for $A_4 > 0$, the frequency of the mode ω_p^{10} increases with increasing A_4, but for $A_4 < 0$, the behavior of ω_p^{10} on A_4 depends on the electron density. If our calculation would be an exact procedure, i.e., it would be possible to include all the exchange-correlation processes in the ground state, as well as in the response and include all modes, all the curves plotted in Fig. 12(b) must be identical at $A_4 = 0$.

Our calculations show how the *free* oscillating states (modes) of the nonparabolic QWW shift their frequencies in dependence on the type and strength of the nonparabolicity. As long as the confining potential is symmetric, *all* antisymmetric modes become dipole active. FIR transmission spectra show all these antisymmetric collective intersubband resonances even at $q_x = 0$, i.e., for perpendicularly incident light without a grating coupler. Hence, the mode spectrum contains for parabolic and nonparabolic QWW's the same modes, shifted only slightly, i.e., the mode spectrum is *universal*, but the FIR spectrum of a nonparabolic QWW shows peaks at ω_p^{10}, ω_p^{21}, ω_p^{30}, ω_p^{32}, ... in difference to the FIR spectrum of a parabolic QWW, which has only the fundamental peak at ω_p^{10}.

It is seen that deviations from the perfect parabolic potential have an appreciable influence on the Q1D plasmons. These imperfections cannot be the source of additional modes. But the nonparabolicity of the confining potential, which breaks Kohn's theorem, shifts the mode frequencies, has a measurable influence on the range of existence $(\omega, q_x, n_{1\mathrm{DEG}})$ of a definite mode and makes all the antisymmetric modes dipole active, i.e., they become observable with perpendicularly incident FIR light.

V. SUMMARY

In this work, we have studied the changes that different types of nonparabolicity of the bare confining potential induce on the dispersion relations of plasmons in quantum-well wires. Assuming spatial symmetric corrections to the bare perfect parabolic potential described by terms of fourth and sixth power, two types of modes oc-

cur, symmetric modes connected with collective electron transitions between states having the same parity and antisymmetric modes connected with collective electron transitions between states with opposite parity. For a bare perfect parabolic potential, the self-consistent calculations of the ground-state and the response show that the so-called fundamental or Kohn's mode ω_p^{10} has a frequency identical with the bare harmonic oscillator frequency, independent from the electron density, if the wave vector is zero. In this case, according to the generalized Kohn's theorem, this mode is connected with the center-of-mass motion of the confined electrons, all the other modes are connected with the relative motion of the confined electrons. Finite wave vectors and nonparabolicity of the bare confining potential of the QWW's break Kohn's theorem and hence, deviations in the spectrum of the Q1D plasmons occur.

(i) For small electron densities, the nonparabolicity can shift the mode ω_p^{10} to larger and smaller frequencies in comparison to the bare harmonic oscillator frequency Ω.

(ii) With increasing density, the frequency of the fundamental mode ω_p^{10} increases.

(iii) The higher modes $\omega_p^{L+1,L}$ are also shifted to higher or smaller frequencies in dependence on the shape of the nonparabolic corrections.

(iv) There are no additional modes as well as mode crossing or anticrossing behavior, induced by the nonparabolicity of the bare confining potential.

Our self-consistent calculations of the ground state in the Hartree approximation and the response in the RPA explicitely show the cancellation of the corrections to the single-particle energy spacing by the Hartree potential $(\Omega - \Omega_{10})$ with the depolarization term of the response Δ_p^{10}.

ACKNOWLEDGMENT

L.W. gratefully acknowledges financial support by the Deutsche Forschungsgemeinschaft (DFG), Project No. We 1532/3-2.

[1] Y.C. Lee, S.E. Ulloa, and P.S. Lee, J. Phys. C **16**, L995 (1983).
[2] S. Das Sarma and W.Y. Lai, Phys. Rev. B **32**, 1401 (1985).
[3] W. Que and G. Kirczenow, Phys. Rev. B **37**, 7153 (1988).
[4] W. Que and G. Kirczenow, Phys. Rev. B **39**, 5998 (1989).
[5] Q. Li and S. Das Sarma, Phys. Rev. B **40**, 5860 (1989).
[6] W. Que, Phys. Rev. B **43**, 7127 (1991).
[7] Q.P. Li and S. Das Sarma, Phys. Rev. B **43**, 11 768 (1991).
[8] L. Wendler, R. Haupt, and R. Pechstedt, Phys. Rev. B **43**, 14 669 (1991).
[9] R. Haupt, L. Wendler, and R. Pechstedt, Phys. Rev. B **44**, 13 635 (1991).
[10] L. Wendler, R. Haupt, and R. Pechstedt, Surf. Sci. **263**, 363 (1992).
[11] L. Wendler and R. Haupt, in *Quantum Effect Physics, Electronics and Applications*, edited by K. Ismail, T. Ikoma, and H.I. Smith, IOP Conf. Proc. No. 127 (Institute of Physics and Physical Society, Bristol, 1992), Chap. 2, p. 51.
[12] L. Wendler, V.G. Grigoryan, and R. Haupt, Superlatt. Microstruct. **12**, 501 (1992).
[13] L. Wendler and V.G. Grigoryan, Phys. Status Solidi B **181**, 133 (1994).
[14] L. Wendler and V.G. Grigoryan, Phys. Rev. B **49**, 14 531 (1994).
[15] W. Hansen, M. Horst, J.P. Kotthaus, U. Merkt, Ch. Sikorski, and K. Ploog, Phys. Rev. Lett. **58**, 2586 (1987).
[16] F. Brinkop, W. Hansen, J.P. Kotthaus, and K. Ploog, Phys. Rev. B **37**, 6547 (1988).
[17] T. Demel, D. Heitmann, P. Grambow, and K. Ploog, Phys. Rev. B **38**, 12 372 (1988).
[18] U. Merkt, Superlatt. Microstruct. **6**, 341 (1989).
[19] T. Egeler, G. Abstreiter, G. Weimann, T. Demel, D. Heitmann, P. Grambow, and W. Schlapp, Phys. Rev. Lett. **65**, 1804 (1990).
[20] T. Demel, D. Heitmann, P. Grambow, and K. Ploog, Phys. Rev. Lett. **66**, 2657 (1991).
[21] A.R. Goñi, A. Pinczuk, J.S. Weiner, J.M. Calleja, B.S. Dennis, L.N. Pfeiffer, and K.W. West, Phys. Rev. Lett. **67**, 3298 (1991).
[22] H. Drexler, W. Hansen, J.P. Kotthaus, M. Holland, and S.P. Beaumont, Phys. Rev. B **46**, 12 849 (1992).
[23] A.R. Goñi, A. Pinczuk, J.S. Weiner, B.S. Dennis, L.N. Pfeiffer, and K.W. West, Phys. Rev. Lett. **70**, 1151 (1993).
[24] A. Schmeller, A.R. Goñi, A. Pinczuk, J.S. Weiner, J.M. Calleja, B.S. Dennis, L.N. Pfeiffer, and K.W. West, Phys. Rev. B **49**, 14 778 (1994).
[25] R. Strenz, U. Roßkopf, F. Hirler, G. Abstreiter, G. Böhm, G. Tränkle, and G. Weimann, Semicond. Sci. Technol. **9**, 399 (1994).
[26] G. Hertel, H. Drexler, W. Hansen, A. Schmeller, J.P. Kotthaus, M. Holland, and S.P. Beaumont, Solid-State Electron. **37**, 1289 (1994).
[27] T. Demel, D. Heitmann, P. Grambow, and K. Ploog, Superlatt. Microstruct. **9**, 285 (1991).
[28] W. Hansen, in *Quantum Coherence in Mesoscopic Systems*, Vol. 254 of *NATO Advanced Studies Institute, Series B: Physics*, edited by B. Kramer (Plenum, New York, 1991), p. 23.
[29] P. Ruden and G.H. Döhler, Phys. Rev. B **27**, 3547 (1983).
[30] L. Brey, N.F. Johnson, and B.I. Halperin, Phys. Rev. B **40**, 10 647 (1989).